Periodic Potentials in One Dimension

Harold V. McIntosh
Departamento de Aplicación de Microcomputadoras,
Instituto de Ciencias, Universidad Autónoma de Puebla,
Apartado postal 461, 72000 Puebla, Puebla, México.

December 20, 2000

Abstract

As part of a collection of samples illustrating the use of the second order real differential equation solver SERO, some variants on the theme of periodic potentials are discussed. Constructing the stability chart for a periodic potential is one of the most important uses of the program, although details of specific solutions are also frequently called for.

Contents

1 Introduction

Periodic potentials can be described in two contexts, classical and relativistic. In each category there is a wide assortment of actual potentials, but in both cases three stand out for their simplicity and generality.

In the Kronig-Penney model [4], the potential starts out as a step function, alternating between one value in part of a unit cell, but another for the rest of the cell. The advantage lies in having a plane wave in each interval, requiring only some trigonometry to match the boundaries and derive energy levels and band structures.

However, these authors noticed that the algebra could be simplified still further when the potential was very large over a limited interval, allowing it to be approximated by a Dirac delta function. In physical terms, the particle receives a pair of jolts as it passes a certain point, one accelerating it and the other slowing it down again. Or the reverse, if the sign of the potential is changed.

Finally, the third choice avoids a potential with discontinuities; a simple periodic function such as the cosine can be selected. Classically, this leads to Mathieu's equation, which has been extensively studied in various places for a variety of reasons; for example, after separation of variables for wave equations in elliptical coordinates [1, 2, 3].

1.1 Schrödinger equation

A 2×2 matrix notation is admirably suited for discussing one-dimensional problems. For the Schrödinger equation, we would write

$$\frac{d\mathbf{Z}(x)}{dx} = \begin{pmatrix} 0 & V(x)-E \\ 1 & 0 \end{pmatrix} \mathbf{Z}(x) \tag{1}$$

taking $\mathbf{Z}$ as a matrix containing two the linearly independent solutions as its columns.

For a constant potential it is a matter of finding the eigenvalues and eigenvectors of the coefficient matrix, then writing the solution as an exponential. Even so, there is a question of keeping the solution in a real form, making it convenient to distinguish $V > E$ with a matrix of hyperbolic functions from the realm $V < E$ with sines and cosines. After introducing the attenuation factor

$$\kappa = (V-E)^{1/2}, \tag{2}$$

the solution takes the form

$$\mathbf{Z}(x) = \begin{pmatrix} \cosh\ \kappa(x-x_0) & \kappa \sinh \kappa(x-x_0) \\ (1/\kappa)\ \sinh\ \kappa(x-x_0) & \cosh\ \kappa(x-x_0) \end{pmatrix} \mathbf{Z}(x_0). \tag{3}$$

Otherwise the wave number $k = i\kappa$ would be used, after switching over to trigonometric functions:

$$\mathbf{Z}(x) = \begin{pmatrix} \cos\ k(x-x_0) & -k \sin k(x-x_0) \\ (1/k)\ \sin\ k(x-x_0) & \cos\ k(x-x_0) \end{pmatrix} \mathbf{Z}(x_0). \tag{4}$$

Splitting a nominal period of 2π into parts and multiplying the matrices corresponding to each part gives a result which could be graphed as a function of the parameters involved. Consider a one dimensional lattice whose base potential is zero, but for which part of the period consists of a

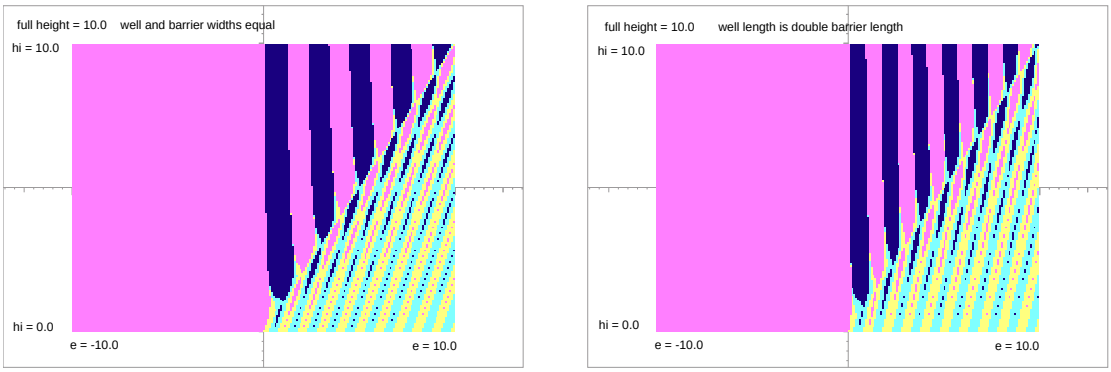

Figure 1: SERO results showing dispersion contours for two Walsh function potentials. Left: well and barrier widths equal. Right: well twice the length of the barrier.

barrier of height hi. In other words, the potential could be a Walsh function of simple form. The result of varying the height from the value of 0.0, representing a plane wave to 10.0, representing a sizable barrier, is shown in Figure 1. Actually it contains contour maps of the dispersion relation

$$\cos\ \theta \quad = \quad \frac{1}{2}\mathrm{Trace}(\mathbf{Z}_{\mathrm{low}}(\alpha)\mathbf{Z}_{\mathrm{high}}(2\pi-\alpha)) \tag{5}$$

as a function of energy and the Walsh function amplitude for a fixed splitting of a period.

The expected result is that for energies larger than the barrier height, the solutions are mostly free waves, with occasuional exponential regions which can be attributed to Bragg reflection. On the other hand, for lower values of the energy the solution resembles bound states confined to the wells with a meagre possibility of tunneling between them, while the diffraction diminishes in intensity the further one goes above the top of the well.

Suppose that V is large with $x - x_0$ proportionally small, keeping $P = V \times (x - x_0)$ constant. Then $\kappa(x - x_0)$ would be infinitesimal with a huge κ, whose reciprocal would remove the lower left element in the solution while cancelling the hyperbolic sine in the upper right element, finally leaving the factor P (remember that κ is only the square root of V). Altogether the solution matrix over such an interval is a shear:

$$\mathbf{Z}(x) \quad = \quad \begin{pmatrix} 1 & P \\ 0 & 1 \end{pmatrix} \mathbf{Z}(x_0). \tag{6}$$

In the context of the Schrödinger equation, it alters the derivatives of wave functions while preserving their continuity.

Joined to an interval of length L, the resulting solution is

$$\begin{pmatrix} 1 & P \\ 0 & 1 \end{pmatrix} \begin{pmatrix} \cosh\ \kappa L & \kappa\ \sinh\ \kappa L \\ (1/\kappa)\ \sinh\ \kappa L & \cosh\ \kappa L \end{pmatrix} = \\ \begin{pmatrix} \cosh\ \kappa L + (P/\kappa)\ \sinh\ \kappa L & \kappa\ \sinh\ \kappa L + P \cosh\ \kappa L \\ (1/\kappa)\ \sinh\ kx & \cosh\ kx \end{pmatrix} \tag{7}$$

The quantities of interest in this new matrix are still its eigenvectors and eigenvalues, and in particular whether the eigenvalues are hyperbolic or trigonometric. Half the trace of the matrix

compared to unity tells which; we get

$$\cosh\ \theta \quad = \quad \cosh\ \kappa L + \frac{P}{2\kappa} \sinh\ \kappa L. \tag{8}$$

Written with wave numbers to orient the interpretation towards free particles rather than bound states,

$$\cos\ \theta \quad = \quad \cos\ kL + \frac{P}{2k} \sin\ kL. \tag{9}$$

this is precisely the dispersion relation obtained by Kronig and Penney. Note that $\sin x/x$ is unity at the origin, gradually diminishing as x increases while retaining the higher zeroes of $\sin\ x$. It is also interesting that the sign of P could be changed, the result being a complementary spectrum. In other words, a series of delta-wells can restrain particles and produce reflections just as well as a series of delta-barriers. The effect carries over to even a single delta-potential.

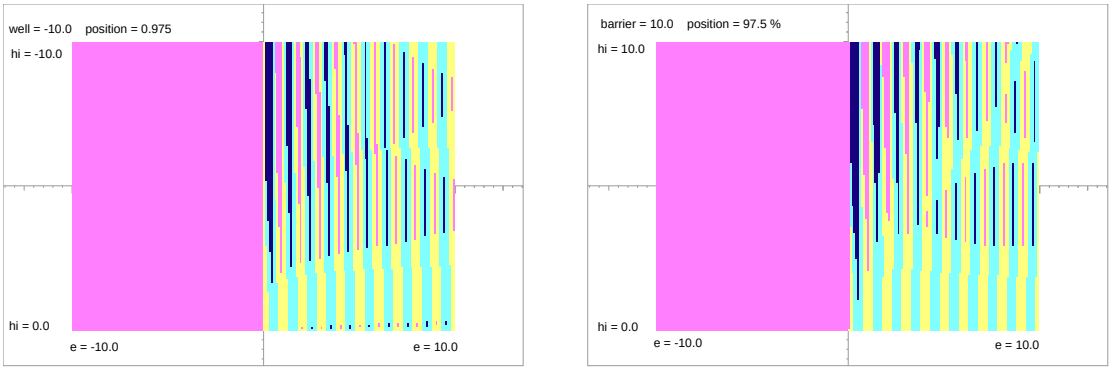

Figure 2: SERO results showing dispersion contours for two Kronig-Penney potentials. Left: wells under a zero floor. Right: barriers above the floor. The incipient delta-function takes up only 2 1/2 percent of the period. The strong moiré effect is the result of pixel size in the graphing program; nevertheless it still mirrors changes in the underlying graph because it is sensitive to the overall widths of the bands being displayed.

The dependence of the dispersion relation on P becomes evident when it is graphed. When P is zero, there is nothing but a plane wave, which is still mostly true when P is small. But when L corresponds to about half a free particle's wave length, there is an amplitude change resulting from a slight reflection, which is compounded as more and more unit cells are taken into account.

At the other extreme, a favorable phase relation allows consistent tunneling from one side of the potential step to the other, making a wave propagate. The size of P, which determines the scale of the effect, is measured by the same scale in which E or V themselves are expressed.

All these relationships can be discerned in Figure 2 on the left, in the regime of wells, interference creates narrow reflection bands wherein waves do not propagate. On the right in the regime of barriers, narrow tunneling bands permit wave propagation. The bands are not always so narrow, and are somewhat complementary, so the two figures look rather much the same. More resolution and enlarging the area under examination would be required to pursue the subject in greater detail.

If the contour maps are examined is closer detail, as in Figure 3, the "bound state" of the Kronig-Penney wells is visible. As the well becomes narrower, it has to become deeper to support a bound state, and thus will show up at an ever higher location in the contour plot as the delta-function limit is taken.

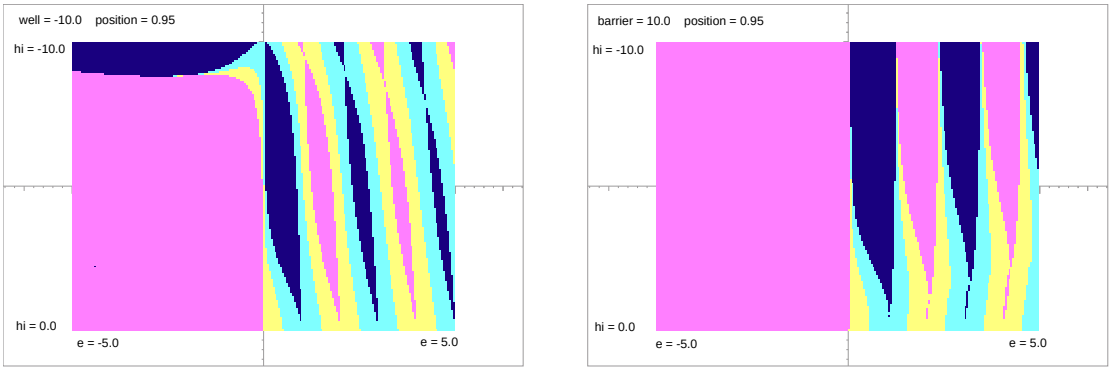

Figure 3: Enlargements of portions of Figure 2.

A third approach to the study of periodic potentials is to use a trigonometric function rather than a Walsh function for the potential of the Schrödinger equation. The solution involves the Mathieu functions, which have been well studied, but for which there are no limits which simplify the algebra as there were for the Kronig-Penney lattices.

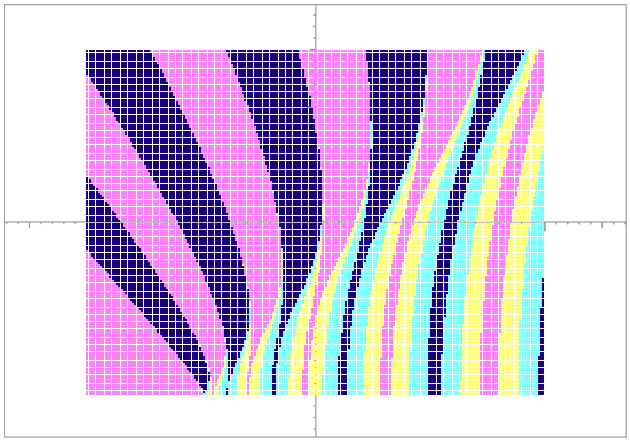

Figure 4: Stability contours for the Mathieu potential.

Figure 4 shows the contour map for the Mathieu dispersion relation, otherwise known as its stability chart. The energy runs from -10.0 to 30.0, the amplitude of the cosine from 0.0 to 15.0. Here the potential is centered on zero, so there are negative energy bound states for sufficiently deep potentials. The Mathieu function itself is traditionally defined in terms of $(\cos\ x + 1)$ to give it a zero floor.

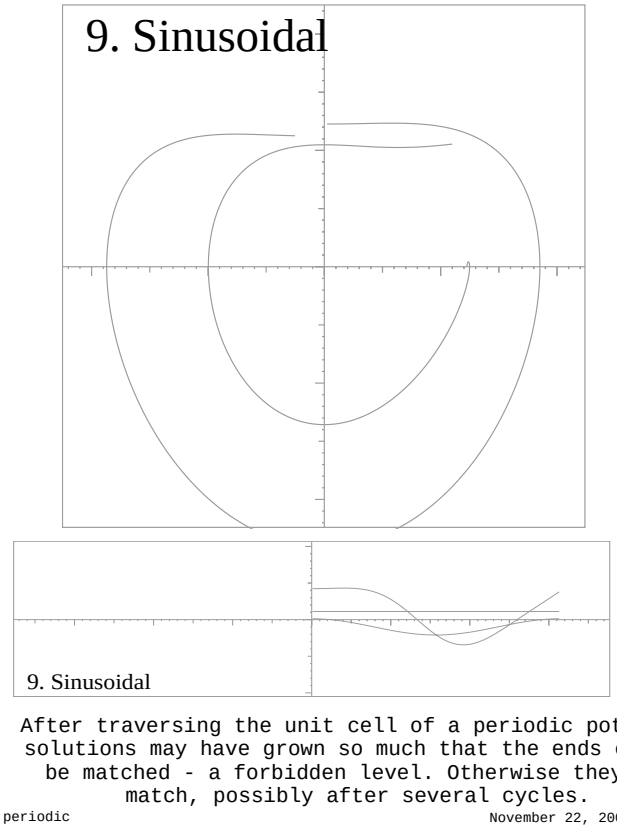

Figure 5: SERO results illustrating a periodic potential.

The program SERO calculates solutions for second order ordinary differential equationa or, equivalently, pairs of first order equations. The latter is the form already taken by the Dirac equation, so it is only necessary to write the coefficient matrix before proceding.

The program has a fixed list of potentials, with provision for varying some of their parameters. After they have been chosen, the solutions can be displayed in one or the other of two forms. One, the more traditional presentation, graphs solutions as functions of the independent variable, sometimes several at a time along with coefficients from the matrix in the form of options.

The other presentation is via the phase plane, wherein one component of the solution is plotted as a function of the other (often, its dertivative).

A sample of the two forms of presentation is shown in Figure 5. They are little used in this report, to get the illustrations for which an independent facility graphing selected dispersion relations has been used.

1.2 Dirac equation

The one-dimensional Dirac equation for a particle of rest mass m_0 has a matrix form

$$\frac{d\mathbf{Z}(x)}{dx} = \begin{pmatrix} 0 & m_0 - (V(x) - E) \\ m_0 + (V(x) - E) & 0 \end{pmatrix} \mathbf{Z}(x). \tag{10}$$

which is structurally somewhat different from the Schrödinger equation because of the symmetric term depending on the rest mass, and the antisymmetric presence of the kinetic energy in two different places.

The substitutions

$$\kappa = [m_0^2 - (V - E)^2]^{1/2}, \qquad \sigma = \left(\frac{m_0 - (V - E)}{m_0 + (V - E)}\right)^{1/2} \tag{11}$$

lead to the same form of solution matrix as before,

$$\mathbf{Z}(x) = \begin{pmatrix} \cosh\ \kappa x & \sigma\ \sinh\ \kappa x \\ (1/\sigma)\ \sinh\ \kappa x & \cosh\ \kappa x \end{pmatrix} \mathbf{Z}(x_0), \tag{12}$$

but still only for a constant energy difference $E - V$. Otherwise the derivative of $V(x)$ would have to be taken into account, introducing additional terms into the coefficient matrix.

When the rest mass is zero, the coefficient matrix is a scalar multiple of the unit antisymmetric matrix, so the use of the angle

$$\varphi = \int_{x_0}^{x} (V(t) - E)dt \tag{13}$$

gives simply

$$\mathbf{Z}(x) = \begin{pmatrix} \cos\ \varphi & -\sin\ \varphi \\ \sin\varphi & \cos\ \varphi \end{pmatrix} \mathbf{Z}(x_0), \tag{14}$$

Irrespective of either m_0 or E, if V is very large yet extending over a small interval such that $V \times (x - x_0) = P$, the result is this same rotation matrix, now running through the angle P. An interesting consequence is that strengths differing by 2π make identical changes to the solution.

The fact that a concentrated potential produces a finite rotation rather than a shear is somewhat disconcerting, since it implies a discontinuity in both components of a solution vector. But mainly, this illustrates the fact that not all potentials give rise to continuous derivatives, nor even to continuous wave functions.

Following the Kronig-Penney precedent of compounding the delta-function potential with a plane wave, we would get

$$\begin{pmatrix} \cos\ P & -\sin\ P \\ \sin\ P & \cos\ P \end{pmatrix} \begin{pmatrix} \cosh\ \kappa L & \sigma\ \sinh\ \kappa L \\ (1/\sigma)\ \sinh\ \kappa L & \cosh\ \kappa L \end{pmatrix} = \begin{pmatrix} \cos(P)\cosh(\kappa L) - (1/\sigma)\sin(P)\sinh(\kappa L) & \sigma\cos(P)\sinh(\kappa L) - \sin(P)\cosh(\kappa L) \\ \sin(P)\cosh(\kappa L) + (1/\sigma)\cos(P)\sinh(\kappa L) & \cos(P)\cosh(\kappa L) + \sigma\sin(P)\sinh(\kappa L) \end{pmatrix} \tag{15}$$

with the dispersion relation

$$\cosh(\theta) = \cos(P)\cosh(\kappa L) + \frac{1}{2}(\sigma - \frac{1}{\sigma})\sin(P)\sinh(\kappa L). \tag{16}$$

This is the spherical cosine law for a unit hyperboloid with an angle between edges of the triangle of $\cosh(\gamma) = \frac{1}{2}(\sigma - 1/\sigma)$. We don't see such clear bumps on the cosine curves as for the Schrödinger equation, but the result is very similar.

2 Small mass compared to height

When the mass is small or even zero, the coefficient matrix of the Dirac equation is nearly a scalar multiple of the unit antisymmetric matrix $\mathbf{i}$. Accordingly solutions take the form seen in Equations (13) and (13). For the potential $A \sin x$ the results for the interval $0 - 2\pi$ are

$$\begin{aligned} \varphi &= \int_0^{2\pi} (A\sin(t) - E)dt \\ &= [-A\cos(t) - Et]_0^{2\pi} \\ &= -2\pi E \end{aligned} \tag{17}$$

and accordingly

$$\mathbf{Z}(2\pi) = \begin{pmatrix} \cos(2\pi E) & -\sin(2\pi E) \\ \sin(2\pi E) & \cos\,(2\pi E) \end{pmatrix} \mathbf{Z}(0), \tag{18}$$

half of whose trace is $\cos(2\pi E)$, independently of the strength of the potential, and even of its form so long as it is periodic. This is evident in Figure 6 and even in the contour plot of Figure 7, whose apparent structure is more likely due to the precision of the computation than to the effects of mass, height, and energy.

Mass and energy may be separated in the Dirac equation by writing the coefficient matrix as $M = A + B$ where $A = (V - E)\mathbf{i}$ and $B = m_0\mathbf{j}$. Factoring the solution into $\mathbf{Z} = \mathbf{UV}$ and solving

$$\frac{d\mathbf{U}}{dx} = (V - E)\mathbf{iU} \tag{19}$$

to get the result already shown in Equation 18 (where the solution was called $\mathbf{Z}$), there remains the solution of the equation for $\mathbf{V}$,

$$\frac{d\mathbf{V}}{dx} = \mathbf{U}^{-1}m_0\mathbf{jUV} \tag{20}$$

When m_0 is small, it is approximately solved by the so-called first Born approximation

$$\mathbf{V}(x) = \mathbf{I} + m_0 \int_0^x \mathbf{U}(t)^{-1}\mathbf{jU}(t)dt + \ldots \tag{21}$$

$$= \mathbf{I} + m_0 \int_0^x \mathbf{jU}^2(t)dt + \ldots, \tag{22}$$

the second form being due to the anticommutation of the quaternion matrices. Taking into account that $\mathbf{U}$ is a combination of $\mathbf{1}$ and $\mathbf{i}$ while the integral is a mixture of $\mathbf{j}$ and $\mathbf{k}$, changes in the dispersion relation due to a small mass will be of at least second order.

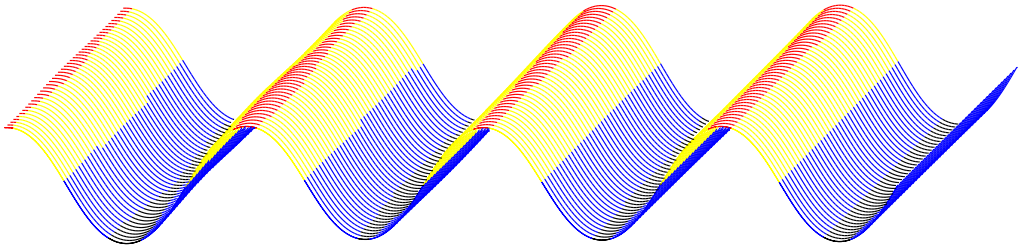

Figure 6: A perspective view of the stability function for the relativistic Mathieu potential. Mass = 0.125, nearly negligible. Strength = 1.0. The energy varies from 0.0 to 3.5, the height of the potential form 0.0 to 1.5. Negative energies give the same results as positive energies. The mass causes a slight expansion of the interval $-1.0-1.0$ occupied by the massless half trace, something visible in the change of coloring.

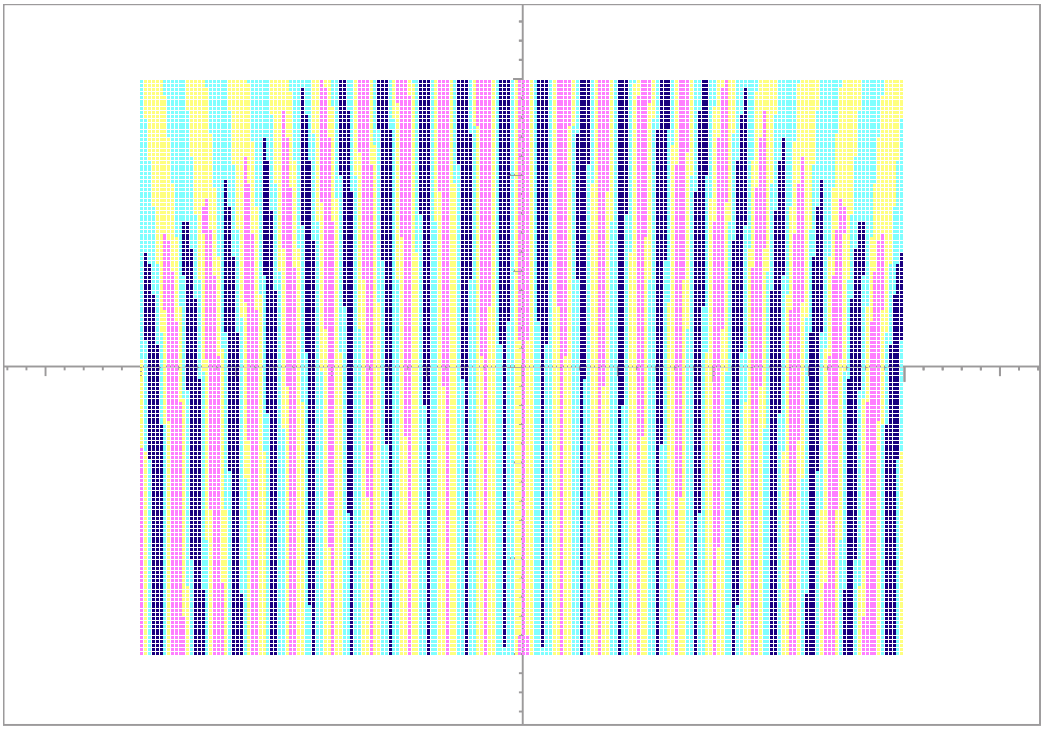

Figure 7: Stability contours for the relativistic Mathieu potential. There is essentially no variation with respect to the height of the potential, with results very close to those for a mass of exactly zero.

3 Mass comparable to height

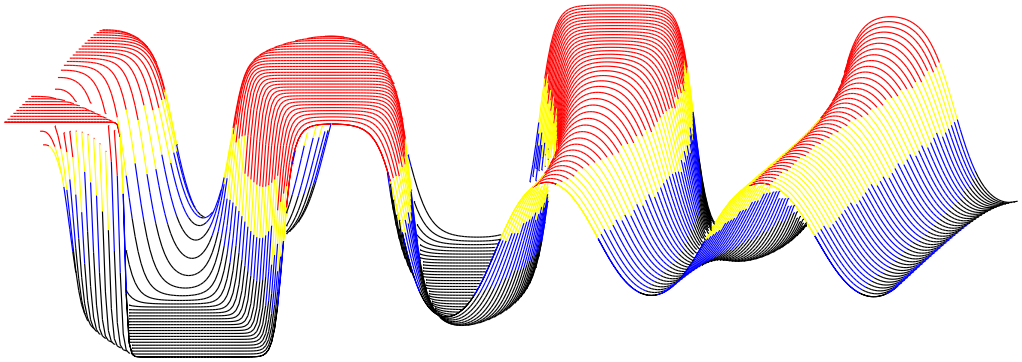

Figure 8: A perspective view of the stability function for the relativistic Mathieu potential. Extreme values have been flattened to make the figure more legible. mass = 1.0, already fairly strong. Strength = 1.0.

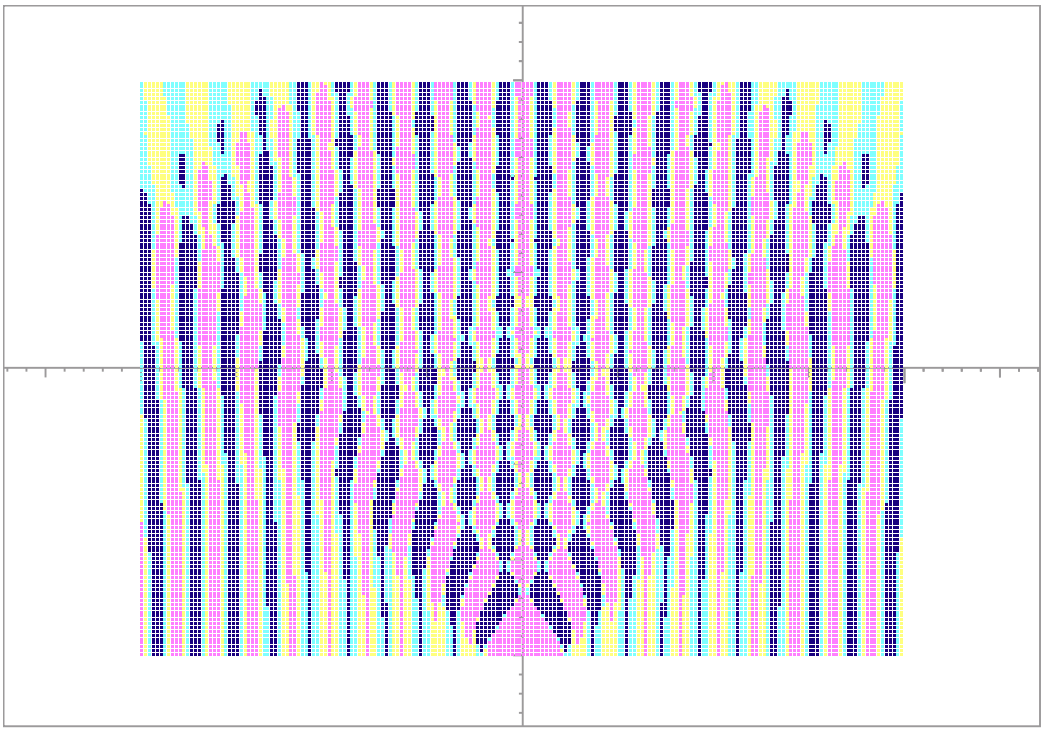

Figure 9: Stability contours for the relativistic Mathieu potential.

4 Mass overwhelms height

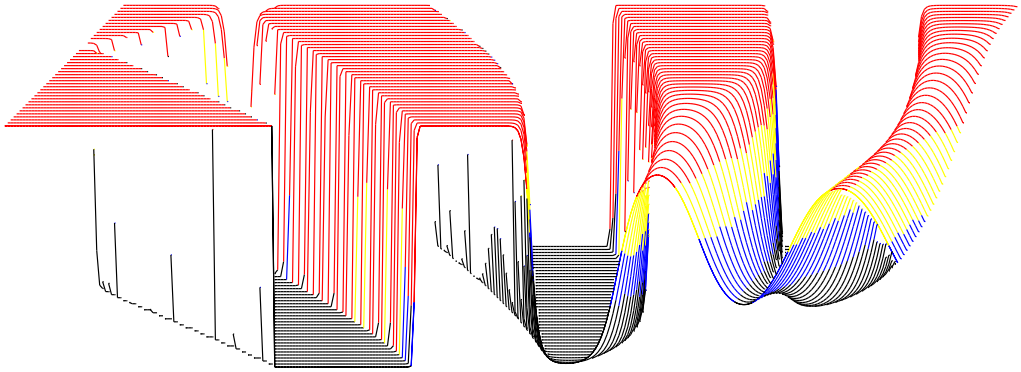

Figure 10: A perspective view of the stability function for the relativistic Mathieu potential. Extreme values have been flattened to make the figure more legible. mass = 1.75, now quite strong. Strength = 1.0.

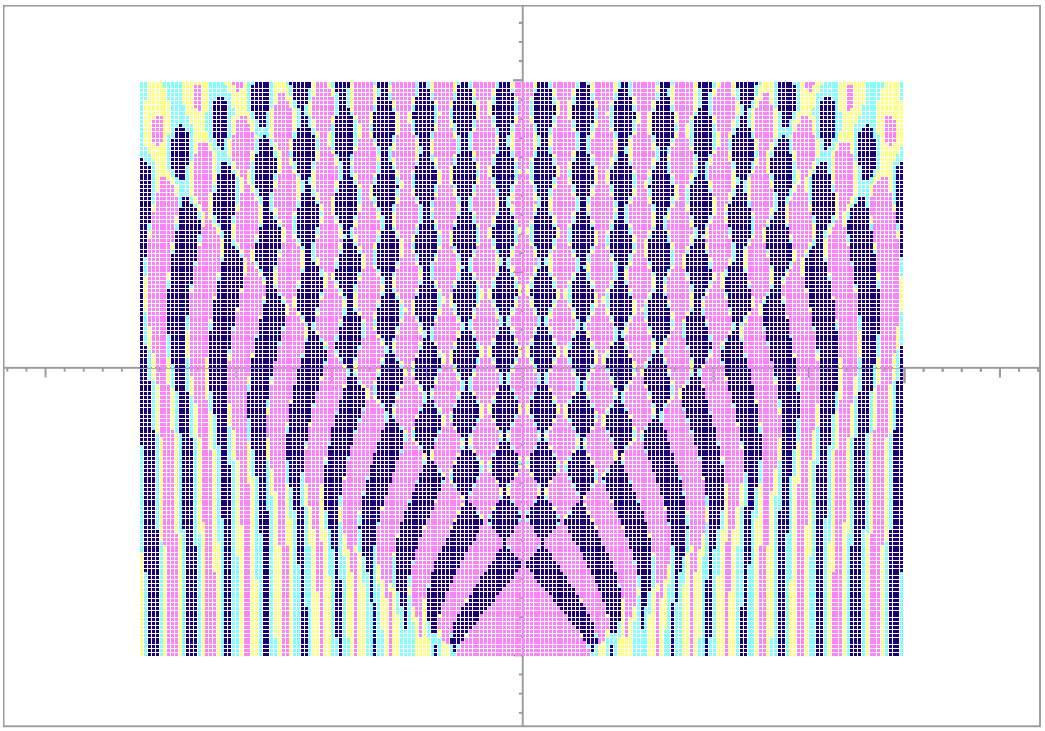

Figure 11: Stability contours for the relativistic Mathieu potential.

5 Further variants

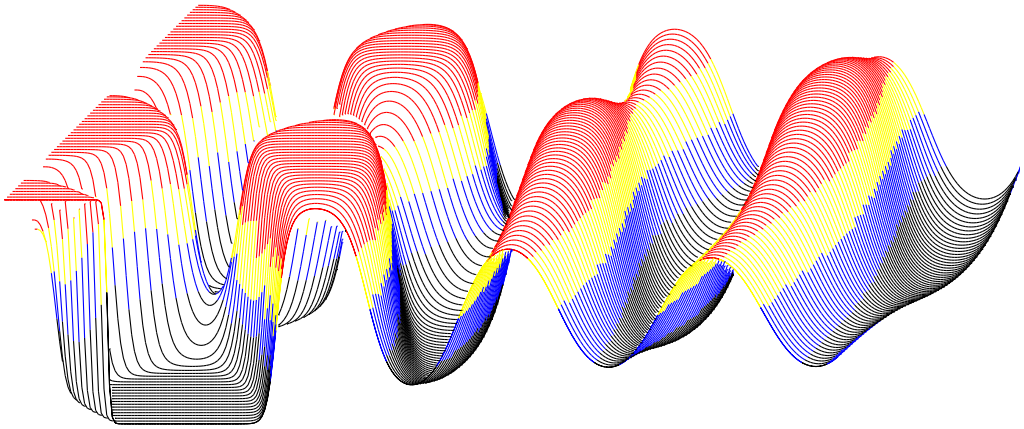

Figure 12: Stability surface for the relativistic Mathieu potential with a sharpening third harmonic.

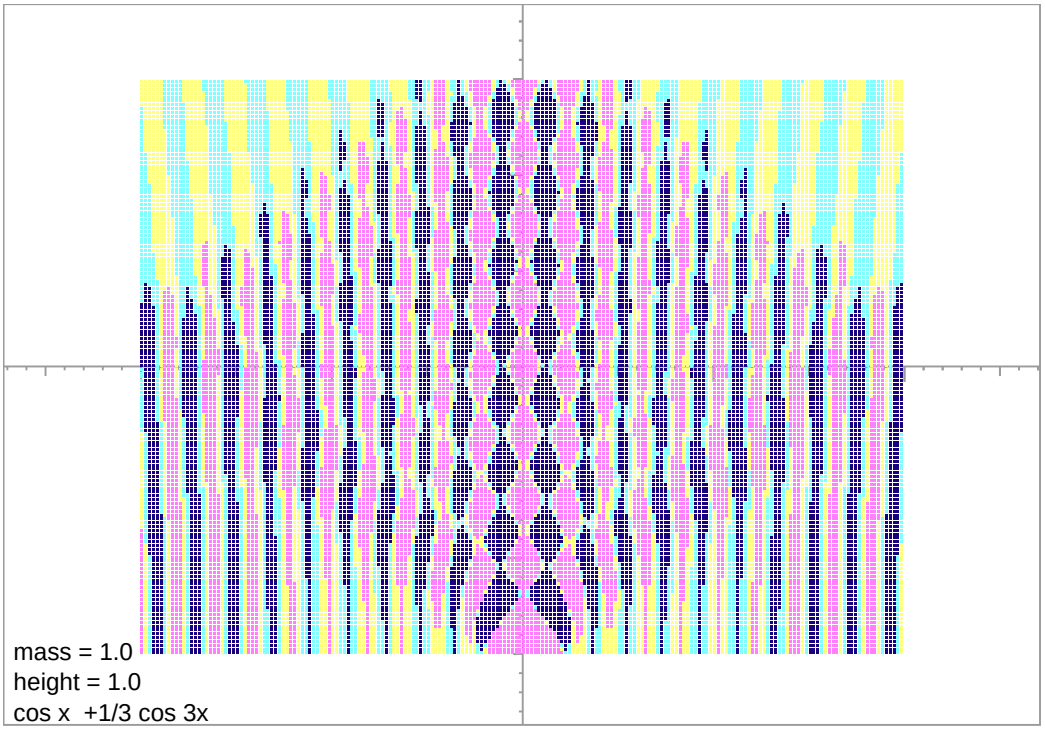

Figure 13: The relativistic Mathieu potential sharpened by its third harmonic.

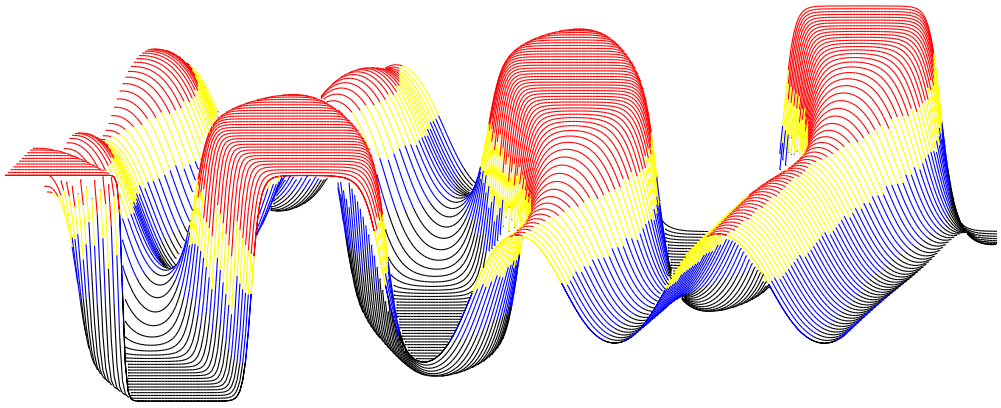

Figure 14: Stability surface for the relativistic Mathieu potential with a flattening third harmonic.

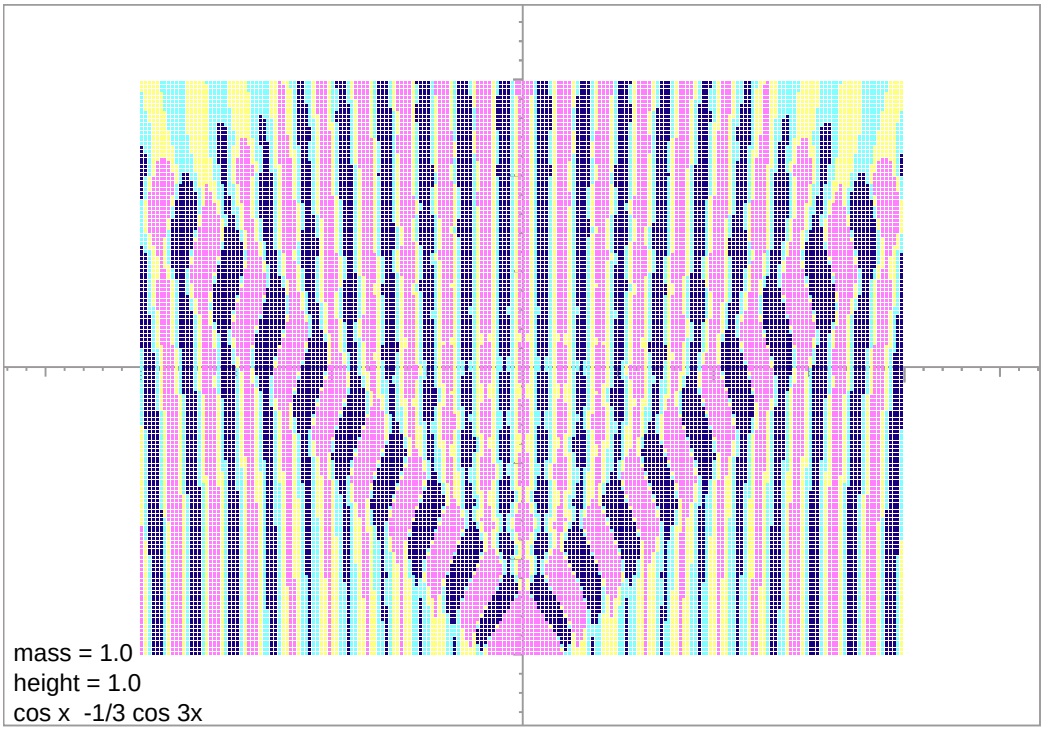

Figure 15: The relativistic Mathieu potential flattened by its third harmonic.

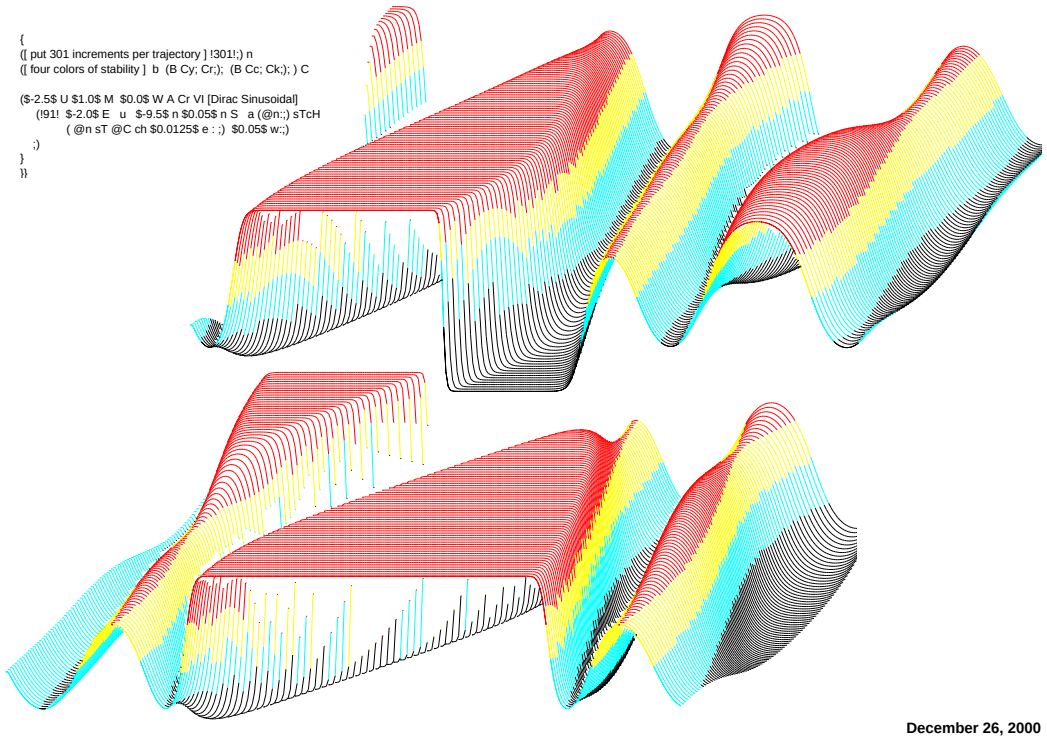

Figure 16: Stability surface for the relativistic Mathieu potential with a delta-function-approximating potential $\cos(x) + \frac{1}{2}\cos(2x) + \frac{1}{3}\cos(3x)$.

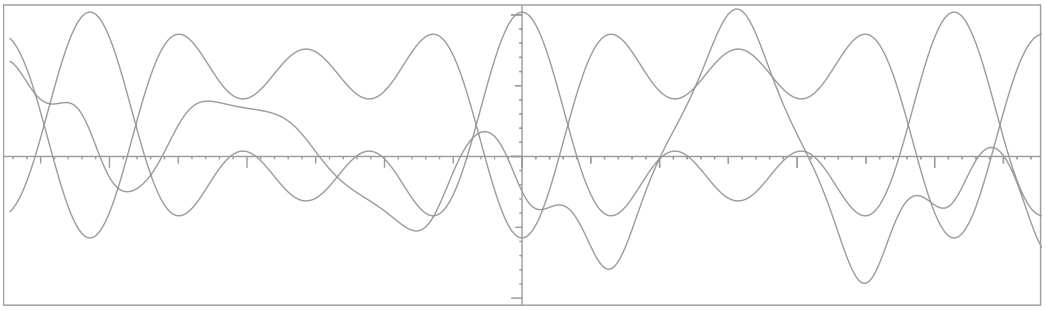

Figure 17: Terms in the coefficient matrix plus one solution for the potential $\cos(x) + \cos(2x) + \cos(3x)$. The potential is fairly flat on the bottom with a dent, while on top the peak approximating the delta function is quite conspicuous. The result is that negative energy solutions see a mild reflecting corrugation while positive energy solutions see an ever rising barrier through which they can tunnel.

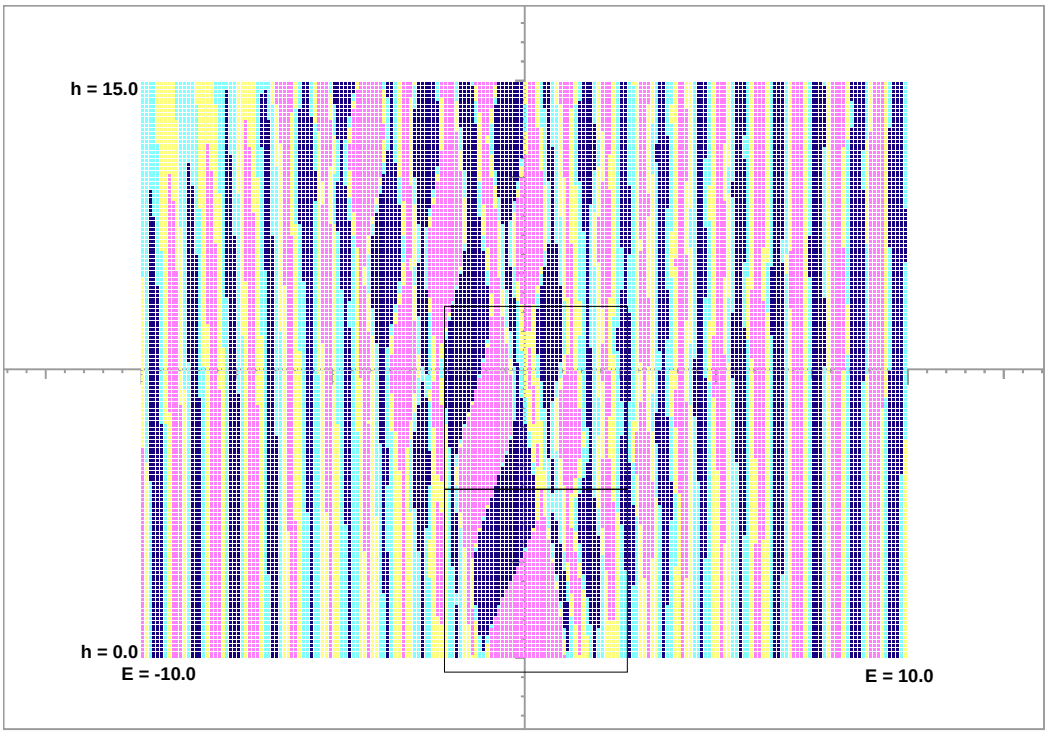

Figure 18: Contour map for the relativistic Mathieu potential with a delta function approximating potential $\cos(x) + \cos(2x) + \cos(3x)$. The squares outline the regions whose perspective view is shown in Figure 16.

Finding a relativistic version of the Kronig-Penney model has created some consternation in the physics literature. The contour map of Figure 18 shows the result of approximating the delta function by the Fourier series $\frac{6}{11}(\cos(x)+\cos(2x)+\cos(3x)+\cdots)$. A notable discrepancy develops between solutions with negative energy and those of positive energy.

Although the average potential in this approximation is zero, it reaches an appreciable maximum while retaining a minimum close to zero. After all, that is the desired result, but the environment which it presents to wave functions of opposite energies is quite different. Instead of a similar mass shell for the two alternatives, the shell has a negligible presence around the high peaks, while constituting a uniform barrier along its base.

The mass-dominated region in Figure 18 rises at a high angle on the left because of the relation of the factor 6/11 in the potential definition to the step size in the contour plotter. effects can be seen on the right but they are barely visible.

6 Summary

In quantum mechanics, periodic potentials are associated with crystal lattices; natural crystals are so large that boundary effects can be ignored, which is not to say that the stydy of crystal surfaces is not important nor that the explicit consideration of boundaries and interfaces is not important. Both possibilities can be given their due recognition in the appropriate places. So considering cyclic or infinite systems is a good place to begin.

Mathematically speaking, the principal difference between the Schrödinger equation for non-relativistic quantum mechanics and the Dirac equation for relativistic quantum mechanics is that large Schrödinger potentials act like shears, while large Dirac potentials acr like rotations. This distinction refers to the action of the coefficient matrix in the system of ordinary differential equations which remains after separating variables in many dimensions or the form which they already have in one dimension.

Large potentials have become involved for historical reasons — symbolic solutions were more tractable the Kronig-Penney model, especially in an era when numerical computation was hard to come by. The Kronig-Penney model gets this simplification from concentrating large potentials in small regions so as to have plane waves elsewhere, both of which are readily soluble.

All seems to have gone well for nonrelativistic applications, but within recent time attempts have been made to get relativistic extensions. Several known aspects of the Dirac equation, such as the zitterbewegung and the Klein paradox, show up in the context of periodic potentials as well. Zitterbewegung and the Foldy-Wouthuysen transformation refer to the construction of positive energy wave packets, which are not of themselves eigenfunctions of the Dirac equation.

The Klein paradox refers to the fact that one and the same eigenfunction can show both positive and negative energy behavior, according to variations in the relationships between mass, kinetic and potential energy from one region to another. In particular, a delta-function potential contains such a reversal of behavior within itself, rotating wave functions in phase space rather than shearing them. In practical terms, they just shift phases, neither binding nor reflecting particles without the collaboration of still further factors.

As the dispersion relations which we have studied show, there are three distinct regions. The first is for energies well above or well below the potentials, including any mass present. In this region the wave function is that of a nearly free particle, with some impediments to propagation resulting from constructive interference of back reflections off potential peaks.

The second region, which is also similar to one of the two classical regions, features exponential behavior of wave functions with the consequent existence of bound states, or greatly suppressed tunneling between nearly bound states. The indicator of this region is the hyperbolic nature of the angle, due to a purely imaginary wave number, for long intervals, interspersed with an actual wave number in shorter intervals.

The new feature, closely related to the Klein paradox, consists of regions in which the particle energy is lower than the potential energy with its mass seell, in some intervals, yet larger than the potential, still including the mass shell, in others. When the minimum of the high shell is greater than the maximum of the low shell, the wave number is never imaginary, but regularly alternates sign. This region is evident in all the examples which have been shown. It is where the would-be delta-spike rotates rather than shears or attenuates.

References

[1] Eugene Jahnke and Fritz Emde, *Tables of Functions with Formulae and Curves*, Dover Publications, New York, 1945. Chapter XI.

[2] E. T. Whittaker and G. N. Watson, *A Course of Modern Analysis*, Cambridge, at the University Press, 1927. Chapter XIX.

[3] Milton Abramowitz and Irene Stgegun (editors), *Handbook of Mathematical Functions*, U. S. Government Printing Office, Washington D. C., 1964. Chapter 20.

[4] R. de L. Kronig and W. G. Penney, "Quantum Mechanics of Electrons in Crystal Lattices," *Proceedings of the Royal Society (London)* **A 130** 499-513 (1931).

[5] W. Kohn, "Analytic Properties of Bloch Waves and Wannier Functions," *Physical Review* **115** 809-821 (1959).

[6] Harold V. McIntosh, "Quantization as an Eigenvalue Problem," In *Group Theory and Its Applications*, Vol. 3, (Ernest M. Loebl Editor), Academic Press pp. 333-368 (1975)

[7] Harold V. McIntosh, "Quantization and Green's Function for Systems of Linear Ordinary Differential Equations," In *Quantum Science: Methods and Structure*, Edited by J. L. Calais, O. Goscinsky. Plenum Press, New York, pp. 227-294 (1976).

[8] Bill Sutherland and Daniel C. Mattis, "Ambiguities with the relativistic delta-function potential," *Physical Review* **A 24** 1194-1197 (1981).

[9] F. Domínguez Adame, "Relativistic and nonrelativistic Kronig-Penney models," *American Journal of Physics* **55** 1003-1006 (1987).

[10] Bruce H. J. McKellar and G. J. Stephenson, Jr., "Klein Paradox and the Dirac-Kronig-Penney model," *Physical Review* **A 36** 2566-2569 (1987).

[11] W. Glöckle, Y. Nogami, and I. Fukui, "Structure of a composite system in motion in relativistic quantum mechanics," *Physical Review* **D 35** 584-590 (1987).

[12] F. A. B. Continho, Y. Nogami, and F. M. Toyama, "General aspects of the bound-state solutions of the one-dimensional Dirac equation," *American Journal of Physics* **56** 904-907 (1988).

[13] F. Domínguez Adame and E. Macía, "On Relativistic Singular Harmonic-Oscillator Potentials," *Europhysics Letters* **8** 711-715 (1989).

[14] F. Domínguez Adame "A generalized Dirac-Kronig-Penney model," *J. Phys Condens. Matter* **1** 109-112 (1989).

[15] F. Domínguez-Adame and E. Maciá, "Bound states and confining properties of relativistic point interaction potentials," *J. Phys. A: Math. Gen.* **22** L419-L423 (1989).

[16] F. Domínguez Adame and M. A. González "Solvable Linear Potentials in the Dirac Equation," *Europhysics Letters* **13** 193-198 (1990).

[17] B. Méndez and F. Domínguez Adame, "A simple numerical method for the determination of relativistic one-dimensional band structures," *J. Phys A: Math. Gen.* **24** L331-L336 (1991).

[18] E. Macía and F. Domínguez Adame, "Scattering states of relativistic point interaction potentials," *J. Phys. A: Math. Gen.* **24** 59-69 (1991).

[19] F. Domínguez Adame, "A relativistic interaction without Klein paradox," *Physics Letters* **A 162** 18-20 (1992).

[20] B. Méndez, F. Domínguez Adame and E. Macía, "A transfer matrix method for the determination of one-dimensional band structures," *J. Phys A: Math. Gen.* **26** 171-177 (1993).

[21] D. W. L. Sprung, Hua Wu and J. Martorell, "Scattering by a finite periodic potential," *American Journal of Physics* **61** 1118-1124 (1993).

[22] S. L. Blundell, "The Dirac Comb and the Kronig-Penney model: Comment on "Scattering from a locally periodic potential," by D. J. Griffiths and N. F. Taussig [Am. J. Phys. 60 883-888 (1992)," *American Journal of Physics* **61** 1147-1148 (1993).

[23] S. H. Patil, "Completeness of the energy eigenfunctions for the one-dimensional δ-function potential," *American Journal of Physics* **68** 712-714 (2000).

[24] D. W. L. Sprung, J. D. Sigetich, Hua Wu and J. Martorell, "Bound states of a finite periodic potential," *American Journal of Physics* **68** 715-722 (2000).

[25] V. Aldaya and J. Guerrero, "Canonical coherent states for the relativistic harmonic oscillator," *Journal of Mathematical Physics* **36** 3191-3199 (1995).

January 11, 2001